Journal of Inorganic and General Chemistry
ZAAC
Zeitschrift für anorganische und allgemeine Chemie
www.zaac.wiley-vch.de
RESEARCH ARTICLE
DOI: 10.1002/zaac.202200344

Special Collection

Lanthanide Complexes (Ln = La, Nd, Dy) of Octaethyl propane-1,1,3,3-tetrayltetrakis(phosphonate): Multidentate Binding Competing with Monodentate DMSO Complexes

Ingo Koehne[a] and Rudolf Pietschnig*[a]

Dedicated to Professor Sjoerd Harder on the Occasion of his 60th Birthday

The preparation of lanthanide nitrate complexes $[Ln(NO_3)_3\{\mathbf{L}\}]_n$ (Ln^{3+} = La, Nd, Dy) supported by the octaethyl propane-1,1,3,3-tetrayltetrakis(phosphonate) (**L**) chelate ligand platform is presented. Re-crystallization of these compounds from DMSO/THF led to a complete replacement of the multidentate phosphonate ester ligand and the formation of exclusively DMSO-supported lanthanide nitrate species $[Ln(NO_3)_3(DMSO)_4]$. The relative basicity of a model phosphonate ester *vs.* DMSO is explored with theoretical means, pointing out the relevance of solvation in this case in line with the experimentally observed exchange process. The optical properties of the dysprosium(III) derivatives are examined in the visible region indicating a significantly higher quantum yield for its tetraphosphonic ester complex than for the DMSO coordinated analog.

Introduction

In the last decades, lanthanide-based materials and compounds have made an important impact as luminescent probes on a variety of technology fields,[1] like organic light-emitting diodes (OLEDs),[1e,2] solar energy conversion,[3] photocatalysis,[4] and life sciences.[5] This is due to their unique spectroscopic properties, such as narrow emission bands, long luminescence lifetimes and large Stokes and/or anti-Stokes shifts.[6] The distinctive split of f-orbitals is rationalized by the electronic configuration of the atoms and their trivalent ions (Ln^{3+}: [Xe] 4f n, n = 0–14).[7] The lanthanide contraction phenomenon (effective ionic-, covalent- as well as van der Waals radii decline stronger than expected from La to Lu) significantly influences metal-ligand bonding as well as intermolecular interactions across the primary- and secondary coordination sphere of the lanthanide center in solid-state and solution, which simultaneously influences structural parameters or lanthanide ion transport properties.[8] With respect to the Laporte selection rule, electronic transitions that maintain parity are forbidden. Thus, electric dipole transitions between multiplets arising from 4f-centered molecular orbitals (MOs) become only allowed if the surrounding environment does not provide inversion symmetry. It is assumed that a Laporte rule violation in such an environment proceeds via an electrostatic crystal field admixture of lanthanide-centered orbitals of even parity (5d, 4f, etc.) to 4f orbitals. Moreover, it is recognized that metal-ligand covalency can also contribute to a 4f shell splitting of lanthanides.[9] In this respect, Hancock & Lee also recently found evidence for the participation of 4f and 5d orbitals in lanthanide metal-ligand bonding.[10] Organic chromophore-supported lanthanide complexes show interesting PL properties due to an enhancement of the f-f-transition luminescence through chemical bonding *via* photo-excitation of the ligand moiety (photo-antenna effect), while the sharp metal-centered emission bands usually occur at the same wavelengths even in case of altered ligand backbones. The ligand platform functions as an energy donor resulting in the overlap of the PL band of the ligand and absorption of the f-f transition for an efficient intramolecular energy transfer.[7] In general, photoluminescent (PL) lanthanide complexes can be roughly characterized by four different types (Chart 1).[6] Type 1 is resembled by (chelate)ligand(s) with a linked but non-coordinative antenna moiety (chromophore). The energy transfer and PL are modulated by interaction between the chromophore and the surrounding analyte. In type 2, the antenna is a part of the (chelate)ligand(s) and participates in coordination of the metal ion. The PL is altered by modulation of a functional group in the ligand's periphery with the analyte. Type 3 is characterized by a coordinating antenna moiety that has no connection to the (chelate)ligand(s). Type 4 is dominated by an unsaturated coordination sphere of the lanthanide ion. The vacant positions are occupied by solvent molecules which are prone to an exchange with analyte molecules causing a modulation of the PL properties. Additional crucial mechanisms causing a change of the PL properties of lanthanide complexes

[a] *Dr. I. Koehne, Prof. Dr. R. Pietschnig*
Institute of Chemistry and Center for Interdisciplinary Nanostructure Science and Technology (CINSaT)
University of Kassel
Heinrich-Plett-Str. 40, 34132 Kassel, Germany
E-mail: pietschnig@uni-kassel.de
Homepage: www.uni-kassel.de/go/hym

Supporting information for this article is available on the WWW under https://doi.org/10.1002/zaac.202200344

This article is part of a Special Collection dedicated to Professor Sjoerd Harder on the occasion of his 60th birthday. Please see our homepage for more articles in the collection.

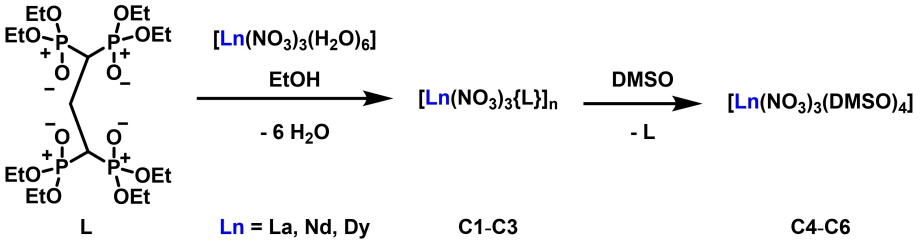

Scheme 1. Preparation of complexes **C1**–**C3** and **C4**–**C6**.

are intramolecular charge transfer (ICT), intramolecular photo-induced electron transfer (PET) as well as luminescence resonance energy transfer (LRET).[6]

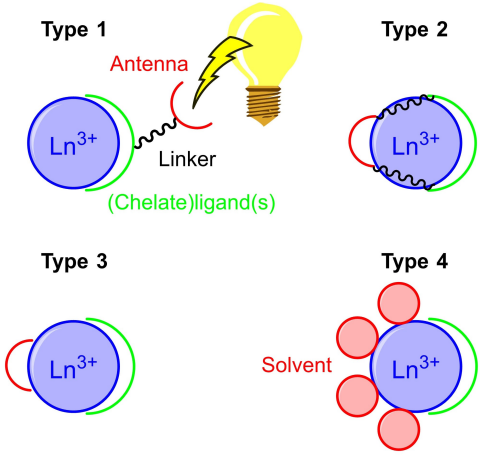

Chart 1. Schematic drawings of four different types (**Type 1-4**) of photoluminescent lanthanide (Ln^{3+}) compounds. **Type1**: (Chelate)ligand and antenna are connected via a linker. Antenna moiety does not coordinate. **Type 2**: Antenna moiety is part of the (chelate)ligand and coordinates. **Type 3**: (Chelate)ligand and antenna moiety are not linked. Antenna molecule coordinates. **Type 4**: Coordination sphere of the lanthanide is not saturated by the (chelate)ligand(s). Vacant positions are occupied by solvent molecules. Adapted from Huang & Huang et al.[6]

In general, phosphates as well as phosphonate ester derivatives are also crucial reagents in spent nuclear fuel (SNF) reprocessing within the nuclear power industry. Tri-*n*-butyl phosphate (TBP) is commonly used to recover Pu(IV) and U(IV) by liquid-liquid extraction (PUREX process) leaving high-level liquid waste (HLLW) that still contains vast amounts of fission products like trivalent actinides (Ac(III)) and lanthanides (Ln(III)). However, before further treatment of HLLW in a partitioning and transmutations (P&T) process, lanthanide species that are considered as neutron poisons need to be separated preventing them from hampering the chain reaction within the P&T process. Besides other, phenanthroline-based bisphosphonate ester derivatives as well as N,O-hybrid ligands like *N*-ethyl-*N*-tolyl-2-amide-1,10-phenanthroline (Et-Tol-PTA) have shown to be suitable ligand platforms for Ac(III) and Ln(III) liquid-liquid separation in recent years.[11]

In comparison to their carboxylic acid congeners, the advantage of phosphonate ester-based organic chromophores grounds on their lower vibrational modes, resulting in mod-erated non emissive excited-state quenching processes and enhanced quantum yields.[12] Our group has focused on mono-, bis- as well as geminal bisphosphonate ester[13] ligand platforms preparing a variety of highly luminescent lanthanide-based MOFs[14] as well as mono- and dimeric lanthanide compounds that exhibit fascinating splitting features in their NIR emission spectra.[15] Here we set out to explore the impact of a fourfold chelating tetraphosphonate ligand.

Results and Discussion

The preparation of complexes $[Ln(NO_3)_3\{\mathbf{L}\}]_n$ (Ln^{3+} = La, Nd, Dy) (**C1**-**C3**) is carried out starting from hexaaqua-trinitrato-lanthanide(III) precursors and the known aliphatic chelate ligand octaethyl propane-1,1,3,3-tetrayltetrakis(phosphonate)[16] (**L**) (Scheme 1). The compounds precipitate from the reaction solution as white, pale pink or pale-yellow solids in good yields between 63–87 %. Identity and purity of the solid products have been established with elemental analysis, IR-spectroscopy, and MALDI-MS. In accordance with a slight weakening of the P< C=>O bond, the $\tilde{\nu}$(P< C=>O) vibration of free **L** (1246 cm^{-1})[13] gets shifted to smaller wavenumbers between 1245 to 1233 cm^{-1} upon coordination to an electronically deficient lanthanide ion in **C1**–**C3** (Table 1). However, the respective $\tilde{\nu}$(P–OEt) stretch is almost unaffected by the coordination process. The most prominent vibrational modes of the nitrate anions are found around 1437–1444 cm^{-1} ($\tilde{\nu}_{N=O}$), 1297–1318 cm^{-1} (asymm. $\tilde{\nu}_{NO2}$) and 1002 cm^{-1} (symm. $\tilde{\nu}_{NO2}$) that are in good agreement with related lanthanide complexes featuring bidentate bound nitrate anions with local C_{2v} symmetry.[17] For a related Ca(II)-complex of ligand **L**, $[CaCl_2\{\mathbf{L}\}]_n$,

Table 1. Selected vibrational modes [cm^{-1}] for **L**, **C1**–**C6** and free DMSO.

Compound	$\tilde{\nu}(NO_3)$	$\tilde{\nu}$(P=O)	$\tilde{\nu}$(P–OEt)	$\tilde{\nu}$(S=O)
L	–	1246	1097	–
C1	1437, 1318, 1002	1245	1101	–
C2	1441, 1297, 1002	1233	1099	–
C3	1444, 1305, 1002	1235	1099	–
DMSO	–	–	–	1042
C4	1436, 1328, 1001	–	–	1025
C5	1438, 1330, 1000	–	–	1025
C6	1470, 1326, 990	–	–	1030

polymeric species in the solid- as well as solution state have been reported.[13] For lanthanide complexes **C1**–**C3**, however, MALDI-MS peaks found at *m/z* = 1439.15 (**C1**), 1443.14 (**C2**) and 1463.14 (**C3**) can be assigned to aggregates of the form $[M(NO_3)_2\{\mathbf{L}\}_2]^+$ which, at least in the gas phase, suggest the presence of monomeric species that carry two neutral ligand molecules **L** per lanthanide ion. In the light of the polymeric nature of the related $[CaCl_2\{\mathbf{L}\}]_n$ compound as well as the poor solubility of **C1**–**C3** in most common solvents, a polymeric structure in the solid-state like depicted in Scheme 1 can be anticipated for **C1**–**C3**.

Compound **C1** is practically insoluble in non-donating NMR solvents like $CDCl_3$ or CD_2Cl_2. Hence, NMR measurements had to be performed in a donating solvent like DMSO-d_6 which exhibits the best solubility. Surprisingly, a comparison between the ^1H, $^{13}C\{^1H\}$ and $^{31}P\{^1H\}$ spectra of **C1** and free **L** reveal no or only neglectable changes upon expected complex formation. Sharp ligand signals are obtained in all NMR spectra of **C1**, but the DMSO-d_6 resonance shows a significant broadening in the ^1H NMR spectrum. This can most likely be attributed to an instant and ready replacement of chelate ligand **L** by DMSO-d_6 molecules upon dissolving and the detection of free **L** in the NMR spectra of **C1** accompanied by $[La(NO_3)_3(DMSO\text{-}d_6)_4]$ species.

Furthermore, a preliminary ^1H DOSY external calibration curve (ECC) molecular weight (*MW*) estimation study of **C1** in DMSO-d_6 also indicates the presence of free **L** and monomeric $[La(NO_3)_3(DMSO\text{-}d_6)_4]$ species in the liquid phase (see ESI, Table S3). The estimated *MWs* of 457 (DSE), 496 (merge) and 569 g/mol (CS) deviate only by 29 (DSE), 19 (merge) and 3% (CS) from **L**'s theoretical *MW* of 588 g/mol. This also indicates free **L** to adopt a compact sphere (CS) shape in solution most preferably.

Attempts to shed light onto the solid-state structures of complexes **C1**–**C3** revealed formation of DMSO-supported lanthanide nitrate compounds and complete replacement of **L**. Vapor diffusion of THF into saturated solutions of **C1**–**C3** in absolute DMSO yielded crystals of the general formula $[Ln(NO_3)_3(DMSO)_4]$ (Ln = La (**C4**), Nd (**C5**), Dy (**C6**)) suitable for SCXRD experiments (Figure 1). Complexes **C4**–**C6** can additionally be prepared by dissolving the above mentioned $[Ln(NO_3)_3(H_2O)_6]$ precursors in absolute DMSO followed by removal of the solvent. As expected, the ^1H and $^{13}C\{^1H\}$ NMR spectra of **C1** show singlet resonances at 2.54 ppm and 40.4 ppm, respectively, corresponding to the methyl groups of the surrounding DMSO donor ligands. The sharp and properly separated resonances additionally indicate a complete absence or an only very slow exchange between DMSO and DMSO-d_6 molecules in solution on the NMR time scale. A separate measurement of neat DMSO in DMSO-d_6 reveals no chemical shift differences between free- and lanthanide-coordinated DMSO molecules. In contrast, the S=O stretches of **C4**–**C6** in a range of 1025 to 1030 cm^{-1} exhibit a significant red shift upon lanthanide ion coordination in comparison to the value obtained for neat DMSO (1042 cm^{-1}) which can again be rationalized by a simultaneous weakening of the S=O bond (Table 1). With exception of **C6** that shows the $\tilde{\nu}_{N=O}$ mode with the highest wavenumber at 1470 cm^{-1} as well as the most red-shifted symmetric $\tilde{\nu}_{NO2}$ vibration at 990 cm^{-1}, the nitrate stretches of **C4**–**C6** are in a comparable range as in **C1**–**C3**.

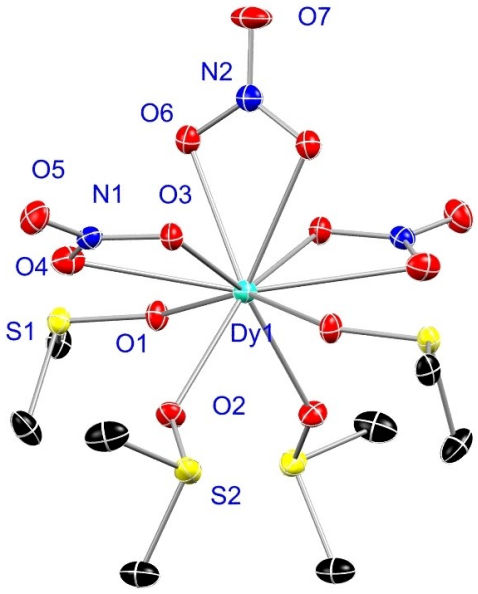

Figure 1. Exemplary crystal structure of complex $[Dy(NO_3)_3(DMSO)_4]$ (**C6**) that is isostructural to those obtained for **C4** and **C5**. Anisotropic displacement parameters are depicted at the 50% probability level. Hydrogen atoms are omitted for clarity. Symmetry transformations used to create equivalent atoms: #1: -x + 1, y, -z + 3/2. Selected structural data are given in Table 2.

Compounds **C1**–**C3** are isostructural crystallizing in the monoclinic space group *C*2/*c*. All compounds feature half a molecule in the asymmetric unit (see ESI, Figures S6-S8). The symmetry equivalent positions are generated *via* a mirror plane. The Ln(III) cations as well as one of the three NO_3^- anions exhibit an occupancy of $^1/_2$. All complexes adopt a doubly-capped square-antiprismatic geometry in a ten-fold all-O coordination around the Ln(III) ion consisting of three bidentate bound nitrate anions as well as four DMSO molecules (Figure 1). Complexes **C1**–**C3** show decreasing $Ln\text{–}O_{(NO3)}$ distances between 2.679(3) Å (**C4**) over 2.622(5) Å (**C5**) to 2.519(2) Å (**C6**) as well as increasing $Ln\text{–}O_{(DMSO/DPSO)}$ bond lengths from 2.471(3) Å in **C4** over 2.414(5) Å in **C5** to 2.320(2) Å in **C6**. Both trends are in accordance with successively decreasing effective ionic radii of the lanthanide ions: La^{3+}(103 pm) > Nd^{3+}(98 pm) > Dy^{3+} (91 pm) (Table 2).[22] The S=O distances are only marginally modulated within the row of compounds **C4**–**C6**, consistent with the observation of similar S=O stretches (see Table 1). The corresponding O–Ln–$O_{(NO3)}$ angles become less acute from **C4** (47.7(9) °) over **C5** (48.6(2) °) to **C6** (48.8(9) °) what again can be explained by successively shrinking effective ionic radii.

Surprisingly, only few other solid-state structures of DMSO- or the closely related diphenyl sulfoxide- (DPSO) supported lanthanide(III) nitrates are available in the literature for comparison. A CCDC search via ConQuest[23] (2022.2.0) lists only five structures with this motif (Table 2): Two $[La(NO_3)_3(DMSO)_4]$

Table 2. Selected bond lengths [Å] and angles [°] of **C4**–**C6** and related complexes **I(Ln)**–**V(Ln)** (Ln = La, Nd, Dy). If there is more than one value for a considered bond length or angle, merged values are given.

Complex	Ln–$O_{(NO3)}$	Ln–$O_{(DMSO/DPSO)}$	S=O	O–Ln–$O_{(NO3)}$
C4	2.679(3)	2.471(3)	1.518(3)	47.7(9)
C5	2.622(5)	2.414(5)	1.519(5)	48.6(2)
C6	2.519(2)	2.320(2)	1.520(2)	48.8(9)
I(La)[18]	2.65(3)	2.48(3)	1.51(3)	45(3)
II(La)[19]	2.683(5)	2.470(5)	1.515(6)	47.2(2)
III(Nd)[20]	2.66	2.39	1.53	47
IV(Nd)[21]	2.57	2.47	1.51	49
V(Dy)[19]	2.463(5)	2.298(5)	1.507	51.5(3)

Table 3. Calculated *Mulliken* charges for the donor oxygen atom in MPOE ($q(O)_P$) and DMSO ($q(O)_S$) on the respective level indicated.

	*B3LYP/6-311+g***	*B3LYP-D3/ 6-311+g***	*wB97X-D/ 6-311+g***
$q(O)_P$	−0.30	−0.29	−0.26
$q(O)_S$	−0.50	−0.50	−0.50

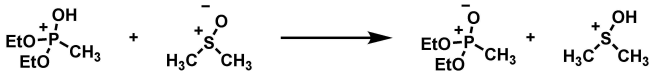

Scheme 2. Calculated proton transfer reaction.

structures can be found, **I(La)**[18] from 1973, and **II(La)**[19] from 1996. Moreover, a $[Nd(NO_3)_3(DMSO)_4]$ (**III(Nd)**)[20] species from 1972 as well as a related diphenyl sulfoxide-supported structure $[Nd(NO_3)_3(DPSO)_4]$ (**IV(Nd)**)[21] from 1986. Unfortunately, there are solely cif-files available for the latter two without further details. Finally, only one dysprosium(III)-based structure $[Dy(NO_3)_3(DMSO)_3]$ (**V(Dy)**)[19] is available from 1996 that carries, in contrast to **C6**, only three DMSO donor molecules. Unlike the 100 K measurements of **C4**–**C6**, the data for all the above-mentioned structures were collected at room temperature.

Comparable trends and magnitudes, like observed for **C4**–**C6**, can be found for bond distances and angles when going from the lanthanum(III) to the dysprosium(III) derivatives in compounds **I(La)**-**V(Dy)**.

The complete displacement of the fourfold chelating ligand **L** by DMSO is somewhat astonishing since for the sulfoxyl- and phosphoryl oxygen atoms similar basicity has been suggested. For DMSO slightly better or similar donor properties than for triethyl phosphate- or phosphane oxides and phosphonates have been reported from solvent- or Co(II) ion extraction studies.[24] However, the basicity of phosphoranyl- and sulfoxyl oxygens is not easy to evaluate, but the ready formation of **C4**–**C6** despite a chelate effect of **L** is possibly due to the large excess of DMSO used as solvent during recrystallization. Using DFT methods, we briefly explored the charge at the oxygen donor atom in DMSO *vs.* methylphosphonic diethyl ester (MPOE), with the latter representing a single out of four donor units in **L**. Using the established basis set *6-311+g*** and functionals with and without dispersive contributions (B3LYP, B3LYP-D3 and wB97X-D) that have been successfully applied in modeling closely related systems,[25] the sulfoxyl oxygen atom in DMSO generally carries a higher negative charge according to the simple Mulliken approach (Table 3), whereas other methods like APT and NBO suggest a more negative charge at the phosphoryl oxygen atom of MPOE (Table S4, ESI). Since charge and basicity are no interchangeable properties, we explored the proton transfer between DMSO and MPOE as a measure for the basicity considering the proton as most simple electrophile (Scheme 2). Here a preference for the protonation at the phosphoryl oxygen atom is observed with $\Delta G = 18.1$ kJ/mol (wB97X-D/*6-311+g***). The corresponding value for $\Delta E = 13.0$ kJ/mol corresponds to the difference of the gas phase proton affinities of the conjugated bases involved, with DMSO showing with 906 the lower gas phase electron affinity than MPOE (919) calculated on wB97X-D/*6-311+g*** level of theory. To probe the effect of solvation single point energies of the species involved in the proton transfer have been computed using the simple polarizable continuum model (PCM) with DMSO as solvent. These results indicate a substantial preference for the DMSO protonation tipping the energetic balance of the reaction shown in Scheme 2 to the right side ($\Delta E = -29.8$ kJ/mol). Although, these computational results will depend on the nature of the *Lewis* acidic partner, they are in good agreement with the experimental outcome in the formation of **C4**–**C6** when solvation is considered.

Photoluminescence properties (PL) of Dy^{3+} compounds C3 and C6

In terms of photoluminescence, lanthanide complexes **C3** and **C6** are best categorized as type 2 and 4 species, respectively (Chart 1). The PL properties of the dysprosium(III) compounds **C3** and **C6** are evaluated in solid-state (Figure 2) as well as in solution ($5x10^{-3}$ mol/L in dry DCM, see ESI: Figures S18 and

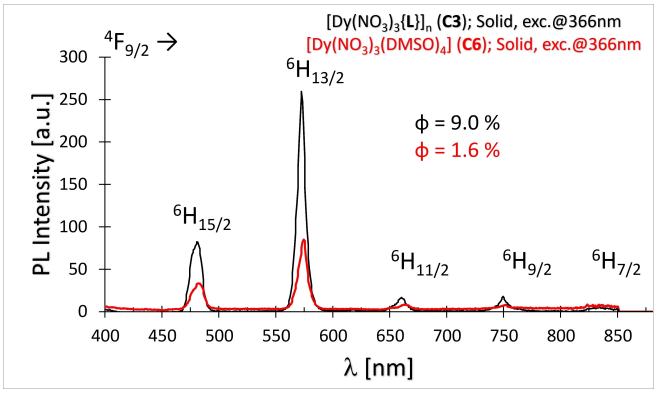

Figure 2. Superimposed room temperature PL emission spectra ($\lambda_{exc.} = 366$ nm) of amorphous solids of the Dy^{3+} complexes **C3** (black) and **C6** (red).

S19). After excitation at 366 nm, Dy^{3+}-centered emissions from the $^4F_{9/2}$ level can be observed around 480 ($\rightarrow{}^6H_{15/2}$), 570 ($\rightarrow{}^6H_{13/2}$), 660 ($\rightarrow{}^6H_{11/2}$), 750 ($\rightarrow{}^6H_{9/2}$) and 840 nm ($\rightarrow{}^6H_{7/2}$), consistent with e.g. other phosphonate ester-supported dysprosium complexes.[15a] Unless amplified by e.g. ligand-to-metal charge transfer (LMCT), the complexes are expected to show no or only very weak metal-centered emissions due to Laporte-forbidden 4f–4f transitions. However, a decent solid-state quantum yield (Φ) of 9.0% for $[Dy(NO_3)_3\{L\}]_n$ (**C3**) not only excludes inversion symmetry for the surrounding coordination sphere of the dysprosium ion, but also attributes the aliphatic chelate ligand **L** with considerable chromophore-like abilities and a photo-antenna effect providing sufficient intramolecular LMCT energy transfer. Compound $[Dy(NO_3)_3(DMSO)_4]$ (**C6**) exhibits diminished PL intensity in combination with a still fair quantum yield of 1.6% in the solid-state. Its solid-state structure does not show inversion symmetry either, but the DMSO donor ligands presumably provide less energy donor abilities and orbital overlap to the metal ion resulting in decreased energy transfer, PL intensity and quantum yield. A similar trend can be derived from the investigations in solution. Here, **L**-based **C3** still shows a fair quantum yield of 1.7% while its DMSO congener **C6** only exhibits a barely detectable quantum yield of 0.1% (see ESI, Figures S18 and S19).

Conclusions

The preparation of three lanthanide complexes $[Ln(NO_3)_3\{L\}]_n$ (Ln^{3+} = La (**C1**), Nd (**C2**), Dy (**C3**)) supported by the aliphatic, tetradentate chelate ligand octaethyl propane-1,1,3,3-tetrayltetrakis(phosphonate) (**L**) is presented. Spectrometric data as well as elemental analysis support the formation of polymeric species in the solid-state. Dissolving **C1** in DMSO-d_6 led to the detection of free **L** *via* a DOSY NMR experiment that is most likely accompanied by $[Ln(NO_3)_3(DMSO\text{-}d_6)_4]$ species. Recrystallization of **C1**–**C3** from DMSO also led to complete displacement of the fourfold chelating tetraphosphonic ester ligand by DMSO molecules resulting in complexes of the general formula $[Ln(NO_3)_3(DMSO)_4]$ (Ln = La (**C4**), Nd (**C5**), Dy (**C6**)). They are comprehensively compared to the few related sulfoxide coordinated lanthanide structures previously reported. While the basicity of phosphoranyl- and sulfoxyl oxygen atoms is not trivial to assess, the ready formation of **C4**–**C6** despite a chelate effect is solvation driven in addition to the large excess of DMSO used as solvent. Evaluation of the photoluminescence (PL) properties of the dysprosium(III) derivatives $[Dy(NO_3)_3\{L\}]_n$ (**C3**) and $[Dy(NO_3)_3(DMSO)_4]$ (**C6**) revealed that especially the **L**-supported **C3** shows reasonable quantum yields in the solid-state (9.0%) as well as in solution (1.7%), which are lost upon replacement of **L** with DMSO ligands. Despite the absence of a chromophore in fourfold chelating ligand **L**, a photo-antenna effect operating via LMCT can be anticipated.

Experimental Section

General Information. Starting materials and solvents were purchased commercially and were used as received, unless stated otherwise. Ligand octaethyl propane-1,1,3,3-tetrayltetrakis(phosphonate) (**L**) was synthesized according to a literature protocol.[16] NMR experiments were performed with Varian 400 or 500 MHz spectrometers, and spectra were processed with MestReNova (v11.0.4-18998, Mestrelab Research S.L.). ^{1}H- and ^{13}C NMR spectra are referenced relative to TMS using the residual solvent signals as internal standards.[26] DOSY-NMR experiments were recorded on a Varian 400 MHz spectrometer. Sample spinning was deactivated during the measurements and the temperature was set and controlled at 298 K. All DOSY experiments were performed using the Dbppste pulse sequence.[27] DOSY transformation and processing was carried out with MestReNova (v11.0.4-18998, Mestrelab Research S.L.). Molecular weight estimation was carried out with the software (v1.3) provided by Bachmann.[28] IR spectra were recorded with a diamond probe ATR IR spectrometer by Bruker. Elemental analyses were performed using a HEKAtech Euro EA-CHNS elemental analyzer. For analyses, samples were prepared in tin cups with V_2O_5 as an additive to ensure complete combustion. MALDI mass spectra were recorded on a Ultraflex TOF device by Bruker Daltonics.

*Synthesis of $[Ln(NO_3)_3\{L\}]_n$ (Ln = La, Nd, Dy) complexes **C1**-**C3**.* **General procedure**: A lanthanide precursor $[Ln(NO_3)_3(H_2O)_6]$ (1.00 mmol) was dissolved in a vial in EtOH (15 mL). Octaethyl propane-1,1,3,3-tetrayltetrakis(phosphonate) (**L**) (589 mg, 1.00 mmol) was diluted with EtOH (15 mL) in a round-bottom flask. The lanthanide precursor solution was added to the ligand solution via syringe and the mixture was stirred at RT overnight (16 h). The formed precipitate was recovered by filtration, washed with small portions of −20 °C EtOH and then pentanes. Air-drying yielded white (La: 0.79 g, 87%), pale pink (Nd: 0.72 g, 78%) or pale-yellow (Dy: 0.59 g, 63%) solids. ***[La(NO$_3$)$_3${L}]$_n$ (C1):*** ^{1}H NMR (500 MHz, DMSO-d_6): δ = 4.11–3.98 (m, 16H, OCH_2CH_3), 3.25 (tt, 2H, $^2J_{PH}$ = 23.5, $^3J_{HH}$ = 6.8 Hz, $CHCH_2CH$), 2.32–2.14 (m, 2H, $CHCH_2CH$), 1.24 (t, 24H, $^3J_{HH}$ = 7.0 Hz, OCH_2CH_3) ppm; ^{13}C{^{1}H} NMR (101 MHz, DMSO-d_6): δ = 62.3 (dd, 8 C, $^2J_{PC}$ = 25.4, $^3J_{PC}$ = 5.7 Hz, OCH_2CH_3), 33.4 (tt, 2 C, $^1J_{PC}$ = 131, $^3J_{PC}$ 7.0 Hz, $CHCH_2CH$), 21.6 (p, 1 C, $^2J_{PC}$ = 4.9 Hz, $CHCH_2CH$), 16.4–16.1 (m, 8 C, OCH_2CH_3) ppm; ^{31}P{^{1}H} NMR (202 MHz, DMSO-d_6): δ = 22.6 (s, 4P) ppm; IR (ATR) $\tilde{\nu}$ = 1437 (N=O), 1318 ($\tilde{\nu}(as)$ NO_2), 1245 (P=O), 1101 (P–OEt), 1002 ($\tilde{\nu}(s)$ NO_2) cm^{-1}; MS (MALDI) m/z (%): 1621.21 (100), 1530.17 (70), 1439.15 (20) [M–NO_3^- + L]$^+$, 1033.08 (50); Elemental analysis calcd (%) for $C_{19}H_{44}LaN_3O_{21}P_4$ (913.36 g/mol): C 24.99, H 4.86, N 4.60; found: C 24.99, H 4.92, N 4.82. ***[Nd(NO$_3$)$_3${L}]$_n$ (C2):*** IR (ATR) $\tilde{\nu}$ = 1441 (N=O), 1297 ($\tilde{\nu}(as)$ NO_2), 1233 (P=O), 1099 (P–OEt), 1002 ($\tilde{\nu}(s)$ NO_2) cm^{-1}; MS (MALDI) m/z (%): 1625.21 (100), 1535.18 (90), 1443.14 (20) [M–NO_3^- + L]$^+$, 1036.08 (80); Elemental analysis calcd (%) for $C_{19}H_{44}NdN_3O_{21}P_4$ (918.70 g/mol): C 24.84, H 4.83, N 4.57; found: C 24.84, H 4.88, N 4.55. ***[Dy(NO$_3$)$_3${L}]$_n$ (C3):*** IR (ATR) $\tilde{\nu}$ = 1444 (N=O), 1305 ($\tilde{\nu}(as)$ NO_2), 1235 (P=O), 1099 (P–OEt), 1002 ($\tilde{\nu}(s)$ NO_2) cm^{-1}; MS (MALDI) m/z (%): 1645.21 (30), 1554.18 (50), 1463.14 (40) [M–NO_3^- + L]$^+$, 1058.08 (100); Elemental analysis calcd (%) for $C_{19}H_{44}DyN_3O_{21}P_4$ (936.96 g/mol): C 24.36, H 4.73, N 4.48; found: C 24.59, H 4.76, N 4.71.

*Synthesis of $[Ln(NO_3)_3(DMSO)_4]$ (Ln = La, Nd, Dy) complexes **C4**–**C6**.* **Method A**: Crystals of **C4**–**C6** suitable for SCXRD measurements were obtained from vapor diffusion of THF into saturated solutions of **C1**–**C3** in absolute DMSO. **Method B**: A lanthanide precursor $[Ln(NO_3)_3(H_2O)_6]$ (5.00 mmol) was dissolved in absolute DMSO (25 mL) in a beaker and stirred at RT for 4 h. To facilitate the removal of access DMSO at the rotary evaporator, toluene was added to form a DMSO/toluene azeotrope. This procedure was repeated several times till a solid was obtained. The solid was additionally washed with toluene (2×), ultimately with pentanes

(2×), and dried under vacuum. Additional drying in a desiccator over $CaCl_2$ for 48 h yielded white (La: 2.49 g, 95%), pale pink (Nd: 2.45 g, 93%) or pale-yellow (Dy: 2.51 g, 92%) solids. ***[La(NO$_3$)$_3$(DMSO)$_4$] (C4):*** ^{1}H NMR (500 MHz, DMSO-d_6): $\delta = 2.54$ (s, 24H, O=S(CH_3)$_2$) ppm; $^{13}C\{^1H\}$ NMR (126 MHz, DMSO-d_6): $\delta = 40.4$ (s, 8 C, O=S(CH_3)$_2$) ppm; IR (ATR) $\tilde{\nu} = 1436$ (N=O), 1328 ($\tilde{\nu}(as)$ NO_2), 1025 (S=O), 1001 ($\tilde{\nu}(s)$ NO_2) cm^{-1}; Elemental analysis calcd (%) for $C_8H_{24}LaN_3O_{13}S_4$ (637.43 g/mol): C 15.07, H 3.80, N 6.59, S 20.12; found: C 15.36, H 3.75, N 6.48, S 20.46. ***[Nd(NO$_3$)$_3$(DMSO)$_4$] (C5):*** IR (ATR) $\tilde{\nu} = 1438$ (N=O), 1330 ($\tilde{\nu}(as)$ NO_2), 1025 (S=O), 1000 ($\tilde{\nu}(s)$ NO_2) cm^{-1}; Elemental analysis calcd (%) for $C_8H_{24}NdN_3O_{13}S_4$ (642.77 g/mol): C 14.95, H 3.76, N 6.54, S 19.95; found: C 15.34, H 3.65, N 6.47, S 20.26. ***[Dy(NO$_3$)$_3$(DMSO)$_4$] (C6):*** IR (ATR) $\tilde{\nu} = 1470$ (N=O), 1326 ($\tilde{\nu}(as)$ NO_2), 1030 (S=O), 990 ($\tilde{\nu}(s)$ NO_2) cm^{-1}; Elemental analysis calcd (%) for $C_8H_{24}DyN_3O_{13}S_4$ (661.03 g/mol): C 14.54, H 3.66, N 6.36, S 19.40; found: C 14.74, H 3.79, N 6.27, S 19.24.

Crystallographic Details. X-ray diffraction experiments were performed with a STOE IPDS 2 with an image plate (Ø 34 cm) using a Mo-GENIX source ($\lambda = 0.71073$ nm). All structures were solved using direct methods (SHELXT)[29] and refined against F^2 using the full-matrix least-squares methods of SHELXL[30] within the SHELXLE GUI[31] or with OLEX2.[32] Additional programs used for structural analysis include Mercury[33] and Platon.[34] CCDC 2212762 (**C4**), 2212763 (**C5**) and 2212764 (**C6**) contain the supplementary crystallographic data for this paper. These data can be obtained free of charge via www.ccdc.cam.ac.uk/data_request/cif.

Computational details. The Gaussian 16 program package was used for all calculations of the computed structures and energies.[35] Geometry optimizations were carried out at the wB97X-D/6-311+G** level of theory. Harmonic vibrational frequency calculations were applied on the fully optimized systems to establish their nature, as characterized by only positive eigenvalues of the Hessian for minima Gibbs free energies were obtained at atmospheric pressure and at 298.15 K utilizing the calculated harmonic frequencies. Solvation effects have been assessed using the polarizable continuum model (PCM), further details are described in the supporting information.

Acknowledgements

The federal state of Hesse, Germany is kindly acknowledged for financial support of the SMolBits project within the LOEWE program. Many thanks to Astrid Pilz for carrying out the X-ray measurements. Open Access funding enabled and organized by Projekt DEAL.

Conflict of Interest

The authors declare no conflict of interest.

Data Availability Statement

The data that support the findings of this study are available in the supplementary material of this article.

Keywords: Coordination Chemistry: O ligands · Lanthanides · Luminescence · Phosphonate esters · Phosphorus · X-ray

[1] a) J.-C. G. Bünzli, S. Comby, A.-S. Chauvin, C. D. B. Vandevyver, *J. Rare Earth* **2007**, *25*, 257–274; b) K. Binnemans, *Chem. Rev.* **2009**, *109*, 4283–4374; c) J.-C. G. Bünzli, S. V. Eliseeva, *J. Rare Earth* **2010**, *28*, 824–842; d) S. V. Eliseeva, J.-C. G. Bünzli, *New J. Chem.* **2011**, *35*, 1165–1176; e) L. Wang, Z. Zhao, C. Wei, H. Wei, Z. Liu, Z. Bian, C. Huang, *Adv. Opt. Mater.* **2019**, *7*, 1801256.
[2] V. V. Utochnikova, in *Handbook on the Physics and Chemistry of Rare Earths, Vol. 59* (Eds.: J.-C. G. Bünzli, V. K. Pecharsky), Elsevier, **2021**, pp. 1–91.
[3] J.-C. G. Bünzli, *Trends Chem.* **2019**, *1*, 751–762.
[4] a) J.-F. Lemonnier, L. Babel, L. Guénée, P. Mukherjee, D. H. Waldeck, S. V. Eliseeva, S. Petoud, C. Piguet, *Angew. Chem.* **2012**, *124*, 11464–11467; *Angew. Chem. Int. Ed.* **2012**, *51*, 11302–11305; b) Y. Zhang, S. Liu, Z.-S. Zhao, Z. Wang, R. Zhang, L. Liu, Z.-B. Han, *Inorg. Chem. Front.* **2021**, *8*, 590–619.
[5] a) S. V. Eliseeva, J.-C. G. Bünzli, *Chem. Soc. Rev.* **2010**, *39*, 189–227; b) J. A. Cotruvo, *ACS Cent. Sci.* **2019**, *5*, 1496–1506; c) S. E. Bodman, S. J. Butler, *Chem. Sci.* **2021**, *12*, 2716–2734.
[6] X. Wang, H. Chang, J. Xie, B. Zhao, B. Liu, S. Xu, W. Pei, N. Ren, L. Huang, W. Huang, *Coord. Chem. Rev.* **2014**, *273–274*, 201–212.
[7] M. Hasegawa, H. Ohmagari, H. Tanaka, K. Machida, *J. Photochem. Photobiol. C* **2022**, *50*, 100484.
[8] K. T. Mahmudov, F. E. Huseynov, V. A. Aliyeva, M. F. C. Guedes da Silva, A. J. L. Pombeiro, *Chem. Eur. J.* **2021**, *27*, 14370–14389.
[9] L. Ungur, B. Szabo, Z. A. Alothman, A. A. S. Al-Kahtani, L. F. Chibotaru, *Inorg. Chem.* **2022**, *61*, 5972–5976.
[10] B. S. Zanella, S. B. Jones, H.-S. Lee, R. D. Hancock, *Inorg. Chem.* **2022**, *61*, 4627–4638.
[11] a) X. Yang, L. Xu, Y. Hao, R. Meng, X. Zhang, L. Lei, Ch. Xiao, *Inorg. Chem.* **2020**, *59*, 17453–17463; b) X.-F. Yang, P. Ren, Q. Yang, J.-S. Geng, J.-Y. Zhang, L.-Y. Yuan, H.-B. Tang, Z.-F. Chai, W.-Q. Shi, *Inorg. Chem.* **2021**, *60*, 9745–9756; c) M. Sun, L. Xu, X. Yang, Sh. Wang, L. Lei, Ch. Xiao, *Inorg. Chem.* **2022**, *61*, 2824–2834.
[12] Y. Hasegawa, Y. Kimura, K. Murakoshi, Y. Wada, J.-H. Kim, N. Nakashima, T. Yamanaka, S. Yanagida, *J. Phys. Chem.* **1996**, *100*, 10201–10205.
[13] I. Koehne, R. Pietschnig, *Eur. J. Inorg. Chem.* **2022**, *2022*, e202200194.
[14] a) K. Krekić, D. Klintuch, R. Pietschnig, *Chem. Commun.* **2017**, *53*, 11076–11079; b) K. Krekić, E. Käkel, D. Klintuch, D. Bloß, R. Pietschnig, *Z. Anorg. Allg. Chem.* **2018**, *644*, 149–154; c) K. Krekić, D. Klintuch, C. Lescop, G. Calvez, R. Pietschnig, *Inorg. Chem.* **2019**, *58*, 382–390.
[15] a) I. Koehne, A. Lik, M. Gerstel, C. Bruhn, J. P. Reithmaier, M. Benyoucef, R. Pietschnig, *Dalton Trans.* **2020**, *49*, 16683–16692; b) I. Koehne, M. Gerstel, C. Bruhn, J. P. Reithmaier, M. Benyoucef, R. Pietschnig, *Inorg. Chem.* **2021**, *60*, 5297–5309; c) M. Gerstel, I. Koehne, J. P. Reithmaier, R. Pietschnig, M. Benyoucef, *Molecules* **2023**, *28*, 48.
[16] G. Sturtz, J. Guervenou, *Synthesis* **1991**, *1991*, 661–662.
[17] A. Cruz-Navarro, J. M. Rivera, J. Durán-Hernández, S. Castillo-Blum, A. Flores-Parra, M. Sánchez, I. Hernández-Ahuactzi, R. Colorado-Peralta, *J. Mol. Struct.* **2018**, *1164*, 209–216.
[18] K. K. Bhandary, H. Manohar, *Acta Crystallogr. Sect. B* **1973**, *29*, 1093–1098.
[19] L. Semenova, B. Skelton, A. White, *Aust. J. Chem.* **1996**, *49*, 997–1004.
[20] L. A. Aslanow, L. I. Soleva, M. A. Porai-Koshits, S. S. Goukhberg, *Russ. J. Struct. Chem.* **1972**, *13*, 655.
[21] G. Fang, C. Benming, L. Yuming, Z. Naijue, Y. Zhaolou, S. Quiang, Z. Quinglian, L. Yuhua, *Chin. J. Struct. Chem.* **1986**, *5*, 109.
[22] R. D. Shannon, *Acta Crystallogr. Sect. A* **1976**, *32*, 751–767.

[23] I. J. Bruno, J. C. Cole, P. R. Edgington, M. Kessler, C. F. Macrae, P. McCabe, J. Pearson, R. Taylor, *Acta Crystallogr. Sect. B* **2002**, *58*, 389–397.
[24] a) R. Shanker, K. S. Venkateswarlu, *J. Inorg. Nucl. Chem.* **1970**, *32*, 229–237; b) S. Banerjee, S. Basu, *Ann. Chim.* **2004**, *94*, 581–590.
[25] A. Orthaber, F. Belaj, R. Pietschnig, *C. R. Chim.* **2010**, *13*, 923–928.
[26] G. R. Fulmer, A. J. M. Miller, N. H. Sherden, H. E. Gottlieb, A. Nudelman, B. M. Stoltz, J. E. Bercaw, K. I. Goldberg, *Organometallics* **2010**, *29*, 2176–2179.
[27] D. H. Wu, A. D. Chen, C. S. Johnson, *J. Magn. Reson. Ser. A* **1995**, *115*, 260–264.
[28] S. Bachmann, B. Gernert, D. Stalke, *Chem. Commun.* **2016**, *52*, 12861–12864.
[29] G. M. Sheldrick, *Acta Crystallogr. Sect. A* **2015**, *71*, 3–8.
[30] G. Sheldrick, *Acta Crystallogr. Sect. C* **2015**, *71*, 3–8.
[31] C. B. Hübschle, B. Dittrich, *J. Appl. Crystallogr.* **2011**, *44*, 238–240.
[32] O. V. Dolomanov, L. J. Bourhis, R. J. Gildea, J. A. K. Howard, H. Puschmann, *J. Appl. Crystallogr.* **2009**, *42*, 339–341.
[33] C. F. Macrae, I. Sovago, S. J. Cottrell, P. T. A. Galek, P. McCabe, E. Pidcock, M. Platings, G. P. Shields, J. S. Stevens, M. Towler, P. A. Wood, *J. Appl. Crystallogr.* **2020**, *53*, 226–235.
[34] A. Spek, *Acta Crystallogr. Sect. D* **2009**, *65*, 148–155.
[35] M. J. Frisch, G. W. Trucks, H. B. Schlegel, G. E. Scuseria, M. A. Robb, J. R. Cheeseman, G. Scalmani, V. Barone, G. A. Petersson, H. Nakatsuji, X. Li, M. Caricato, A. V. Marenich, J. Bloino, B. G. Janesko, R. Gomperts, B. Mennucci, H. P. Hratchian, J. V. Ortiz, A. F. Izmaylov, J. L. Sonnenberg, Williams, F. Ding, F. Lipparini, F. Egidi, J. Goings, B. Peng, A. Petrone, T. Henderson, D. Ranasinghe, V. G. Zakrzewski, J. Gao, N. Rega, G. Zheng, W. Liang, M. Hada, M. Ehara, K. Toyota, R. Fukuda, J. Hasegawa, M. Ishida, T. Nakajima, Y. Honda, O. Kitao, H. Nakai, T. Vreven, K. Throssell, J. A. Montgomery Jr., J. E. Peralta, F. Ogliaro, M. J. Bearpark, J. J. Heyd, E. N. Brothers, K. N. Kudin, V. N. Staroverov, T. A. Keith, R. Kobayashi, J. Normand, K. Raghavachari, A. P. Rendell, J. C. Burant, S. S. Iyengar, J. Tomasi, M. Cossi, J. M. Millam, M. Klene, C. Adamo, R. Cammi, J. W. Ochterski, R. L. Martin, K. Morokuma, O. Farkas, J. B. Foresman, D. J. Fox, Wallingford, CT, **2016**.

Manuscript received: October 28, 2022
Revised manuscript received: December 9, 2022
Accepted manuscript online: December 9, 2022

